2015 IEEE International Conference on Robotics and Automation (ICRA)
Washington State Convention Center
Seattle, Washington, May 26-30, 2015

Modeling and Steering of a Novel Actuated-Tip Needle through a Soft-Tissue Simulant using Fiber Bragg Grating Sensors

Roy J. Roesthuis, Nick J. van de Berg, John J. van den Dobbelsteen and Sarthak Misra

Abstract— **Needle insertions are common during surgical procedures. Accurately delivering the needle at a specific location in the human body is of importance for the clinical outcome of the procedure. Studies have already shown that robotically inserting traditional needles with a bevel tip can improve targeting accuracy. However, steering of such needles requires spinning the needle, which may lead to additional tissue damage. Therefore, we propose a novel design consisting of a flexible needle with a tendon-driven actuated-tip. Changing the orientation of the actuated-tip allows to control the steering direction of the needle and the amount of deflection. We derive the kinematic model which describes the needle path given the actuated-tip orientation based on nonholonomic kinematics. We present a method for steering the needle towards a target location in soft tissue. This method incorporates online parameter estimation in order to adapt for changes in tissue stiffness. Needle insertion experiments are performed in soft-tissue simulants, made from porcine gelatin. Needle tip pose is measured during insertion using Fiber Bragg Grating (FBG) based shape reconstruction. Results show that the needle can be steered towards targets located at 20 mm from the initial insertion axis, at a depth of 100 mm with a mean targeting error of 2.02 mm.**

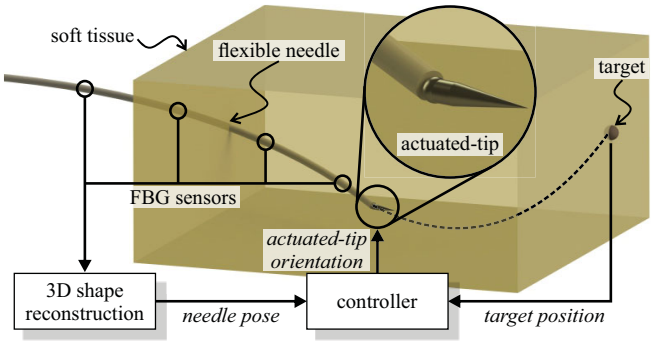

Fig. 1. A flexible needle with a tendon-driven actuated-tip is used to steer towards a desired target in soft tissue. The orientation of the actuated-tip can be controlled, allowing to change the steering direction of the needle during insertion. Fiber Bragg Grating (FBG) sensors along the needle shaft are used to determine needle curvature, from which the three-dimensional (3D) needle shape is reconstructed. Information about needle shape and location of the target is used to determine the orientation of the actuated tip such that the needle is steered towards the target.

I. Introduction

Percutaneous needle insertion is one of the most common minimally invasive surgical (MIS) procedures. As opposed to traditional surgery, MIS aims at minimizing patient trauma, and thereby reducing patient recovery time and patient scarring. Needles are used to reach specific locations in the human body: e.g., for diagnosis and treatment of malignant tissue in the case of biopsies or brachytherapy, respectively. Accurately steering the needle towards the desired location is challenging for a clinician since it can be difficult to predict needle motion. Unexpected changes in the mechanical properties of the tissue can cause the needle to deviate from the intended path. Hence, multiple insertions may be required for a succesful diagnosis or treatment which increases procedure time and patient discomfort.

Over the last decade, several studies have proposed for robotically inserting needles with the goal increasing the targeting accuracy and thereby reducing procedure time [1], [2]. These systems combine medical imaging techniques with models which predict needle motion during insertion. Many studies focus on steering needles with an asymmetric (bevel) tip. Rotation of the needle about its longitudinal axis is used to steer the needle in a desired direction. The curvature of the needle path can be changed by duty cycled spinning of the needle, which enables to steer the needle along a pre-defined path [3], [4]. However, spinning of the needle may lead to additional tissue damage which is not desirable. Therefore, alternative methods for steering needles in soft tissue using novel needle designs have been presented recently. These designs consist of needles in which (parts of) the needle can actively be controlled [5]–[8]. Both Webster *et al.* and Sears and Dupont developed concentric tube robots [5], [6]. These robots consist of telescoping pre-curved superelastic tubes, allowing them to manipulate entire needle shape. However, employing them for use in soft tissue requires a follow-the-leader type of steering, which has not yet been done [9]. More recently, Ko *et al.* presented a bio-inspired needle design (4 mm diameter) consisting of four interlocked segments [7], [8]. This design allows to modify the steering angle by changing the relative offset between the segments and hence, thereby change the curvature of the needle path.

In this work, we present a novel method for steering needles through soft tissue based on a new needle design with an actuated-tip (Fig. 1). This tip is of conical shape and is mounted on a ball-joint. Actuation of the tip by

R.J. Roesthuis and S. Misra are affiliated with the Department of Biomechanical Engineering, MIRA – Institute for Biomedical Technology and Technical Medicine, University of Twente, The Netherlands. S. Misra. is also affiliated with the Department of Biomedical Engineering, University of Groningen and University Medical Centre Groningen, The Netherlands. N.J. van de Berg and J.J. van den Dobbelsteen are affiliated with Biomechanical Engineering (3mE), Delft University of Technology, The Netherlands. This research is supported by the Dutch Technology Foundation STW (H-Haptics Project #12159), which is part of the Netherlands Organization for Scientific Research (NWO) and partly funded by the Ministry of Economic Affairs, Agriculture and Innovation.

four tendons allows to change tip orientation, which enables three-dimensional (3D) steering of the needle through soft tissue without spinning the needle about its longitudinal axis. Compared to earlier needle designs, our design requires only little space in the needle itself, leaving enough space for an inner stylet. We derive the kinematic model for the needle, which describes the needle path through soft tissue given the orientation of the actuated-tip and the forward insertion velocity. A control method is presented for steering the needle towards a target location. A method for online parameter estimation is also presented to allow the controller to adapt for changes in soft-tissue stiffness. Hence, this study aims to contribute to research into needle steering by proposing both a novel needle design, and a model and methods for steering such needles.

We perform needle insertion experiments with a prototype needle (2 mm diameter) in soft-tissue simulants, made from porcine gelatin. The needle is equipped with a nitinol stylet on which an array of Fiber Bragg Grating (FBG) sensors is integrated (Fig. 1). These sensors are used to determine needle curvature, from which needle shape is reconstructed during the insertion procedure [10], [11]. Needle tip pose from the reconstructed shape is used by the steering algorithm to calculate actuated-tip orientation during insertion. First, insertions are performed in order to characterize needle bending for different steering angles and to validate the proposed model. Then, the needle is inserted into a multilayer phantom of varying stiffness to evaluate our method for online parameter estimation. Finally, the needle is steered in 3D towards different target locations.

This paper is outlined as follows: Section II presents the model which describes the needle path based on the actuated-tip orientation and the method for steering the needle towards a target location. The experimental setup and design of the novel needle with actuated-tip are discussed in Section III, where we also describe the method for shape reconstruction using FBG sensors. Section IV presents the results of the insertion experiments. Finally, we conclude the study in Section V where we also provide directions for future work.

II. Modeling and Steering of the Actuated-Tip Needle

This section presents our method of steering the actuated-tip needle to a desired position in soft tissue. First, we derive the kinematic model that describes 3D motion of the actuated-tip needle through soft tissue. Then, we present a method for steering the needle towards a target location.

A. Modeling Insertion of the Actuated-Tip Needle

A flexible needle with a bevel tip deflects from a straight path when it is inserted into soft tissue due to an asymmetric distribution of forces at the tip. Studies have shown that the amount of deflection depends both on needle geometric and material properties, as well as tissue properties [12], [13]. Thin needles deflect more than thicker, rigid needles due to their smaller bending stiffness. Also, needle deflection was shown to increase for tissues with a higher stiffness. Webster

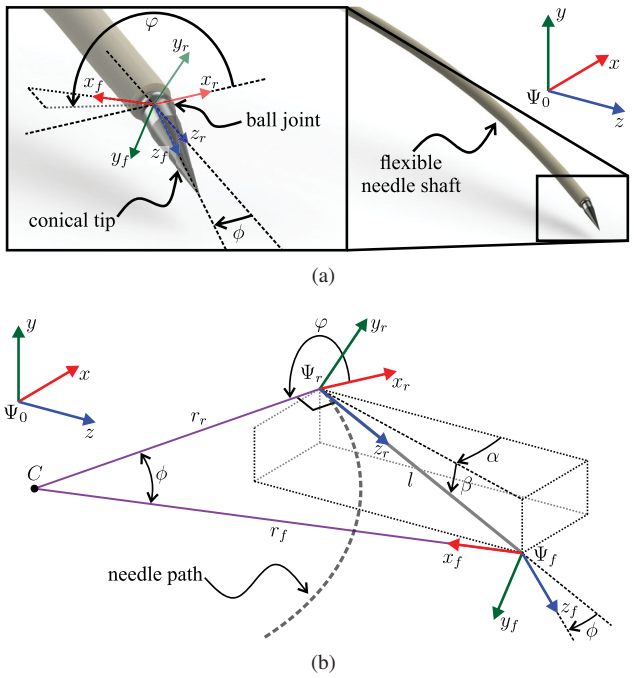

Fig. 2. (a) The actuated-tip needle consists of a flexible shaft and an conical tip. The conical tip is mounted on a ball joint, which enables changing its orientation to a specific direction (φ) at a certain steering angle (ϕ). The orientation of the needle at the tip is denoted by the rear frame (Ψ_r), while the orientation of the actuated-tip is denoted by the front frame (Ψ_f). (b) The needle is assumed to follow a circular path (radius r_r, center C). This radius depends on the actuated-tip steering angle (ϕ) and the offset (l) of the front frame with respect to the rear frame.

et al. demonstrated that the needle path of flexible needles with a bevel tip can be approximated by a constant curvature arc [14]. They derived a model to describe needle motion based on the nonholonomic kinematics of a bicycle with a fixed steering constraint. Ko *et al.* also derived a model of their bio-inspired needle based on nonholonomic kinematics.

Our needle has an actuated-tip which consists of a conical tip mounted on a ball joint (Fig. 2(a)). The orientation of the actuated-tip with respect to the longitudinal axis of the needle determines both the direction of bending and the amount of bending. Actuated-tip orientation is defined by two angles: The first determines the direction of bending (φ), while the amount of bending depends on the steering angle (ϕ). We also assume our needle follows an arc of constant curvature for a fixed steering angle (Fig. 2). We propose a model which assumes kinematics similar to that of a bicycle, for which the radius of the path is determined by the offset (l) of the front frame (Ψ_f) with respect to the rear frame (Ψ_r), and the steering angle (ϕ)

$$r_r = l \Big/ \tan(\phi), \tag{1}$$

where we define the position of the needle tip to be equal to that of the rear frame. The offset (l) depends on the stiffness of the tissue: A low-stiffness tissue results in a large bending radius for a certain steering angle and hence, corresponds to a large offset.

The configuration of the needle at the tip and the orien-

tation of the actuated-tip is fully described by the following generalized coordinates (Fig. 2(b))

$$\boldsymbol{q} = \begin{bmatrix} p^0_{r,x} & p^0_{r,y} & p^0_{r,z} & \alpha & \beta & \varphi & \phi \end{bmatrix}^T, \quad \text{with } \begin{bmatrix} p^0_{r,x} & p^0_{r,y} & p^0_{r,z} \end{bmatrix}^T = \boldsymbol{p}^0_r \in \mathbb{R}^3, \tag{2}$$

where $\boldsymbol{p}^0_r$ is the position of the needle tip relative to the global reference frame (Ψ_0), and α and β describe the orientation of the needle at the tip. Since we do not spin the needle, we do not consider rotation of the needle about its longitudinal axis. Further, φ and ϕ in (2) describe the orientation of the actuated-tip with respect to the orientation of the needle at the tip. The orientation of the needle tip with respect to the global reference frame (Ψ_0) is given by (Fig. 2)

$$\boldsymbol{R}^0_r = \boldsymbol{R}_y(\alpha)\boldsymbol{R}_x(-\beta) \in \mathrm{SO}(3), \tag{3}$$

which consists of a rotation (by α) about the y-axis of the global reference frame, followed by a rotation (of $-\beta$) about the x-axis of the resulting, rotated frame. The orientation of the actuated-tip with respect to the orientation of the needle at the tip is given by (Fig. 2)

$$\boldsymbol{R}^r_f = \boldsymbol{R}_z(\varphi)\boldsymbol{R}_y(\phi) \in \mathrm{SO}(3), \tag{4}$$

which consists of a rotation (by φ) about the z_r-axis, followed by a rotation (of ϕ) about the y-axis of the resulting, rotated frame.

We assume that the tissue surrounding the needle is stiff enough to prevent sideways motion of the needle. Therefore, four Pfaffian constraints exist for the proposed model: The velocities along the x-axis and y-axis of both the rear frame and the front frame are zero (i.e., $\dot{x}_r = 0$, $\dot{y}_r = 0$, $\dot{x}_f = 0$, $\dot{y}_f = 0$). We can write the velocities along the axes of the rear frame (Ψ_r) and the front frame (Ψ_r) as [15]

$$\begin{aligned} \begin{bmatrix} \dot{x}_r & \dot{y}_r & \dot{z}_r \end{bmatrix}^T &= \boldsymbol{R}^r_0 \begin{bmatrix} \dot{p}^0_{r,x} & \dot{p}^0_{r,y} & \dot{p}^0_{r,z} \end{bmatrix}^T, \\ \begin{bmatrix} \dot{x}_f & \dot{y}_f & \dot{z}_f \end{bmatrix}^T &= \boldsymbol{R}^f_0 \begin{bmatrix} \dot{p}^0_{f,x} & \dot{p}^0_{f,y} & \dot{p}^0_{f,z} \end{bmatrix}^T, \\ \text{with } \begin{bmatrix} p^0_{f,x} & p^0_{f,y} & p^0_{f,z} \end{bmatrix}^T &= \boldsymbol{p}^0_f \in \mathbb{R}^3, \end{aligned} \tag{5}$$

where $\boldsymbol{R}^r_0 = (\boldsymbol{R}^0_r)^{-1}$ and $\boldsymbol{R}^f_0 = (\boldsymbol{R}^0_r\boldsymbol{R}^r_f)^{-1}$, and $\boldsymbol{p}^0_f$ the (virtual) position of the front frame. Since the position of the front frame with respect to the rear frame is known, we can rewrite (5) as function of the generalized coordinates. This is used to express the Pfaffian constraints in matrix form as [15]

$$\begin{bmatrix} \dot{x}_r & \dot{y}_r & \dot{x}_f & \dot{y}_f \end{bmatrix}^T = \boldsymbol{A}(\boldsymbol{q})\dot{\boldsymbol{q}} = 0, \tag{6}$$

with $\boldsymbol{A}(\boldsymbol{q}) \in \mathbb{R}^{k \times n}$, and k the number of velocity constraints (i.e., $k = 4$) and n the number of generalized coordinates (i.e., $n = 7$). The kinematic model is given by

$$\dot{\boldsymbol{q}} = \boldsymbol{g_1}(\boldsymbol{q})u_1 + \boldsymbol{g_2}(\boldsymbol{q})u_2 + \boldsymbol{g_3}(\boldsymbol{q})u_3 = \boldsymbol{G}(\boldsymbol{q})\boldsymbol{u}, \tag{7}$$

where the columns ($\boldsymbol{g_1}(\boldsymbol{q})$, $\boldsymbol{g_2}(\boldsymbol{q})$ and $\boldsymbol{g_3}(\boldsymbol{q})$) of $\boldsymbol{G}(\boldsymbol{q})$ are a basis for the null space of matrix $\boldsymbol{A}(\boldsymbol{q})$ in (6). These columns depend on the choice for the inputs (u_1, u_2 and u_3). The

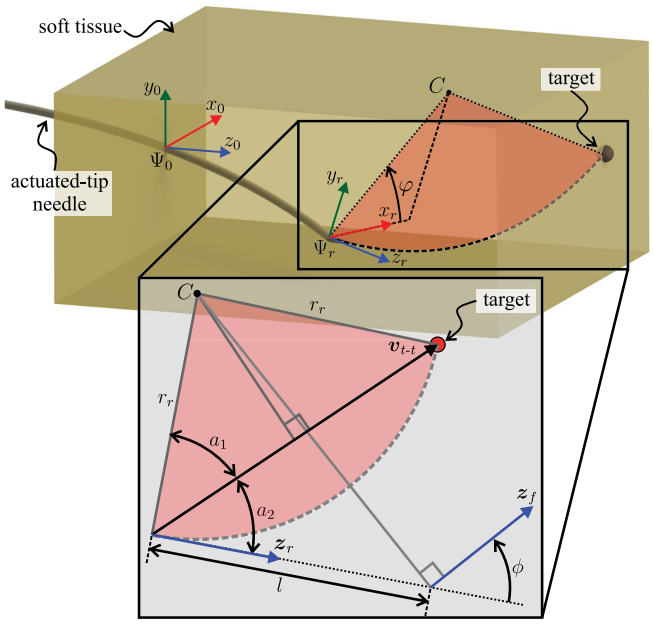

Fig. 3. Schematic representation of the actuated-tip needle being steered through soft tissue towards a target. The dashed curve represents the circular path along which the needle is steered. Given the location of the target with respect to the tip frame (Ψ_r), the actuated-tip steering direction (φ) is determined. The inset shows the bending plane of the needle, from which the steering angle (ϕ) is calculated using the targeting vector ($\boldsymbol{v}_{t\text{-}t}$).

rear frame velocity equals to the insertion velocity of the needle (i.e., $\dot{z}_r = v$), and choosing this for input u_1 gives

$$\dot{\boldsymbol{q}} = \begin{bmatrix} \cos(\beta)\sin(\alpha) \\ \sin(\beta) \\ \cos(\alpha)\cos(\beta) \\ \frac{\cos(\varphi)\tan(\phi)}{l\cos\beta} \\ \frac{\tan(\phi)\sin(\varphi)}{l} \\ 0 \\ 0 \end{bmatrix} v + \begin{bmatrix} 0 \\ 0 \\ 0 \\ 0 \\ 0 \\ 1 \\ 0 \end{bmatrix} \dot{\varphi} + \begin{bmatrix} 0 \\ 0 \\ 0 \\ 0 \\ 0 \\ 0 \\ 1 \end{bmatrix} \dot{\phi}, \tag{8}$$

where it immediately follows that u_2 and u_3 equal the angular speed of the actuated-tip steering direction ($\dot{\varphi}$) and angle ($\dot{\phi}$), respectively. In the next section the model is used to steer the needle towards a desired location in soft tissue.

B. Steering the Actuated-Tip Needle

We aim to steer the needle through soft tissue towards a fixed target location. We assume a constant insertion velocity of the needle (i.e., v = constant). The orientation of the actuated-tip is calculated such that the needle is steered towards the target along a circular path (Fig. 3). We use the needle configuration at the tip (frame Ψ_r) to calculate the steering direction and steering angle of the actuated-tip (i.e., φ and ϕ). The steering direction is calculated using the position of the target in the needle tip frame

$$\varphi = \tan^{-1}\left(t^r_y / t^r_x\right), \tag{9}$$

with $\begin{bmatrix} t^r_x & t^r_y & t^r_z \end{bmatrix}^T = \bar{\boldsymbol{t}}^r \in \mathbb{R}^3$ the target position. Given the needle tip orientation from (3), we calculate the target posi-

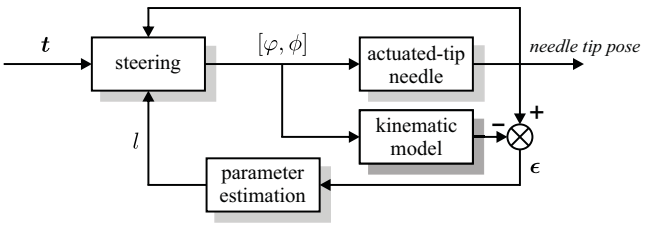

Fig. 4. Needle steering with online parameter estimation. The steering direction (φ) and steering angle (ϕ) of the actuated-tip are calculated given the target location ($\boldsymbol{t}$) and needle tip pose. The difference ($\boldsymbol{\epsilon}$) in needle tip pose is used to estimate the front frame offset (l).

tion in the needle tip frame using the following homogeneous transformation

$$\bar{\boldsymbol{t}}^r = \boldsymbol{H}_0^r \bar{\boldsymbol{t}}^0 = \begin{bmatrix} \boldsymbol{R}_r^{0T} & -\boldsymbol{R}_r^{0T}\boldsymbol{p}_r^0 \\ 0_3^T & 1 \end{bmatrix} \bar{\boldsymbol{t}}^0, \tag{10}$$

with $\boldsymbol{H}_0^r \in \mathrm{SE}(3)$, and $\bar{\boldsymbol{t}}^r$, $\bar{\boldsymbol{t}}^0 \in \mathbb{R}^4$ the homogeneous representation of the target position in the tip frame and in the global reference frame, respectively. The actuated-tip steering angle (ϕ) is solved by considering the two-dimensional bending plane of the needle (Fig. 3). We define the targeting vector ($\boldsymbol{v}_{t-t}$) between the needle tip and the target, which is used to calculate the radius of the circular needle path

$$r_r = \frac{\|\boldsymbol{v}_{t-t}\|}{2\cos(a_1)}, \text{ with } a_1 = \frac{1}{2}\pi - a_2. \tag{11}$$

Taking the dot product between the targeting vector and the unit vector ($\hat{\boldsymbol{z}}_r$) denoting the needle tip frame z-axis gives

$$\boldsymbol{v}_{t-t} \bullet \hat{\boldsymbol{z}}_r = \|\boldsymbol{v}_{t-t}\| \cos(a_2), \tag{12}$$

from which a_2 can be solved. The desired bending radius is calculated using (11), and then the actuated-tip steering angle is calculated from (1).

C. Parameter Estimation

The steering method presented in the previous section requires the front frame offset (l) to be known. As was explained, this offset is related to the tissue stiffness: A large value for the offset corresponds to a tissue with a low stiffness, resulting in a needle path with a large bending radius for a certain steering angle. In order to account for changes in soft-tissue stiffness, we propose a method for online parameter estimation of the front frame offset. This allows to adapt for changes in stiffness of the soft tissue during steering.

During insertion, the inputs to the system are also provided to the kinematic model presented in Section II-A (Fig. 4). The difference ($\boldsymbol{\epsilon}$) between the measured and modeled needle tip pose is then used to estimate the front frame offset. At an instant of time (t) during insertion, the mean-squared-error ($\boldsymbol{\epsilon}_{\text{mse}}$) is determined for a specific window length (W_t)

$$\boldsymbol{\epsilon}_{\text{mse}} = \frac{1}{W_t}\int_{t-W_t}^{t} \boldsymbol{\epsilon}^2 dt. \tag{13}$$

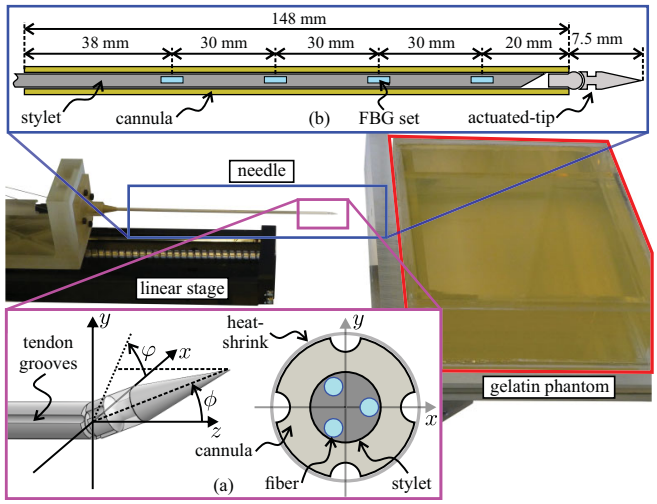

Fig. 5. The experimental testbed consists of a linear stage with a carriage on which the actuated-tip needle is mounted. The carriage holds four motors, which each drive a tendon in order to control the orientation of the actuated-tip. The linear stage enables insertion of the needle into the gelatin phantom. (a) The needle tip has a conical shape and is placed on a ball joint. Four tendons are placed inside grooves (90° spacing) in the cannula (2 mm diameter) and are attached to the tip. These allow to control two degrees-of-freedom: The steering direction (φ) and the steering angle (ϕ). (b) The inner stylet consists of a nitinol wire (1 mm diameter), on which three optical fibers are integrated. These fibers each have an array of four Fiber Bragg Grating (FBG) sensors, spaced 30 mm from each other.

This error is evaluated for different values of the offset, and the minimum is determined using a hill-climbing algorithm and hence, this results in an estimate of the offset.

III. Materials and Methods

This section describes the materials and methods used to steer the actuated-tip needle towards a desired location in a soft tissue simulant. First, we present the design of the novel needle with actuated-tip and the experimental testbed used for steering the needle into a soft tissue simulant. Next, we describe the method for needle shape reconstruction during insertion using strain measurements from FBG sensors.

A. Design of Novel Needle with Actuated-Tip

The design of the novel needle with actuated-tip is schematically shown in Fig. 5. The needle tip has a conical shape with an apex angle of 20° and an approximate length of 5 mm. The tip is placed on top of a ball joint, and actuated by means of four steering tendons working in complementary pairs. Besides the relative tendon motions required to steer the tip, the selection of an overall tendon pretension level allows the adaptation of joint friction, which is required to adjust the mechanism's stiffness. Each of the four tendons are individually driven by a Maxon EC-max 22 motor (Maxon Motor Ag., Sachseln, Switzerland) and allow the tip to rotate with two orthogonal degrees-of-freedom (DOF). These DOF are the steering direction (φ) and the steering angle (ϕ). The entire system is rigidly fixed to a linear stage that realizes the needle insertion and provides a third DOF (Fig. 5). The needle consists of a nitinol stylet with a diameter of 1 mm and a PEEK (Poly-Ether

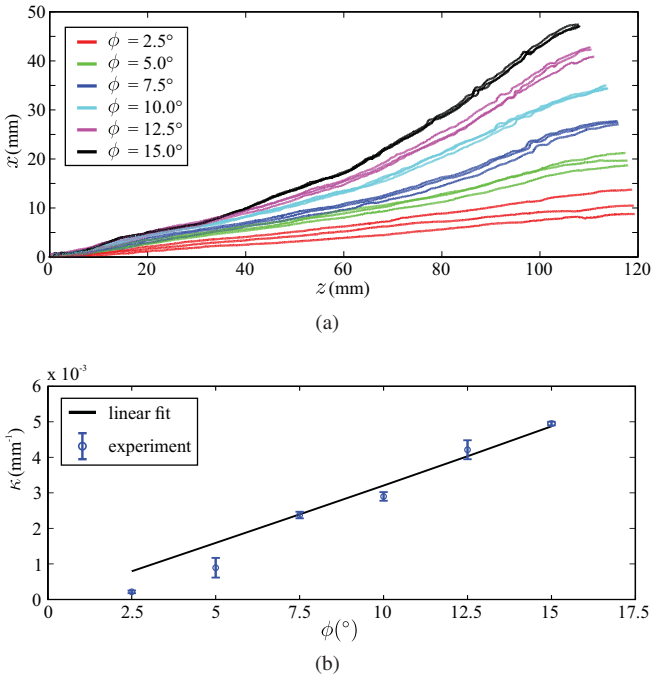

Fig. 6. Characterization of needle bending curvature (κ) for different values of the actuated-tip steering angle (ϕ). (a) Recorded needle tip positions using Fiber Bragg Grating (FBG) based shape reconstruction. Three insertions are performed for each steering angle. (b) Curvature of the needle path for the different steering angles.

Ether Ketone) plastic cannula (IDEX Health & Science, Oak Harbor, USA), with a diameter of 2 mm. This is comparable in size to a 14 gauge needle, which is commonly used for biopsies. A layer of PET plastic (Vention Medical, Salem, USA) heat-shrink tubing covers the cannula grooves and keeps the actuation tendons in place. The outer diameter of the needle is approximately 2 mm. Needle insertions are performed in soft-tissue simulants, which are made from porcine gelatin (Dr. Oetker, Bielefeld, Germany). Increasing the gelatin to water ratio results in stiffer gels.

B. Fiber Bragg Grating-based Shape Sensing

Fiber Bragg Gratings (FBG) sensors can be seen as optical strain gauges: Changes in mechanical strain cause a change of the reflected Bragg wavelength [16]. In earlier studies, we used FBG sensors for shape reconstruction and steering of a bevel tipped needle inside a soft tissue [10], [11]. We have also used them for closed-loop control of a tendon-driven continuum manipulator in free-space [17]. Three optical fibers are integrated in the stylet (Fig. 5(b)), each having an array of four FBG sensors at 30 mm from each other. These FBG sensors are co-located in four FBG sets, which allows to measure the axial strain at three different positions on the cross-section of the stylet. From these strain measurements, the magnitude and the direction of the curvature are calculated upon bending. Information about the curvature along the entire length of the stylet is retrieved by interpolation of the discrete curvature values. Deflection is obtained by integrating the curvature magnitude twice. For more information about the method for shape reconstruction

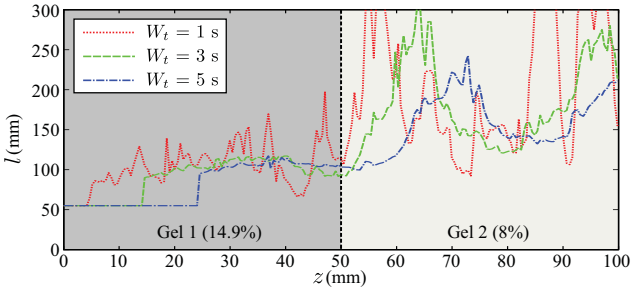

Fig. 7. Online estimation of the front frame offset (l) during insertion into a multilayer phantom for different window lengths (W_t = 1 s, 3 s and 5 s). *The accompanying video demonstrates the results of these parameter estimation experiments.*

we refer to our earlier work [11], [17]. Information about needle tip pose is used during insertion to steer the needle towards a desired location, which is demonstrated in the next section.

IV. Experimental Results

This section presents the experiments performed with the actuated-tip needle. First, experiments are performed in order to characterize the needle bending curvature as a function of the actuated-tip steering angle. Next, we evaluate the algorithm for parameter estimation by inserting the needle into a multilayer phantom with varying stiffness. Finally, the needle is steered towards different target locations.

A. Needle Characterization Experiments

We perform a set of insertion experiments in order to characterize our needle and to validate the model presented in Section II-A. The needle is inserted into a phantom with a amount of gelatin of 14.9% (percentage by weight). This results in a gel with a Young's modulus of 35 kPa, which resembles the stiffness of human breast tissue [18], [19]. The needle is inserted a distance of 120 mm into the phantom with a constant velocity of 5 mm/s for the following steering angles (Fig. 6): 2.5°, 5°, 7.5°, 10°, 12.5° and 15°. The steering direction is the same for all insertions (i.e., $\varphi = 0°$) and three insertions are done for each steering angle. Needle tip position during insertions is determined using FBG-based shape reconstruction (Fig. 6(a)). The curvatures of the needle paths are determined by doing a non-linear least-squares circle fit to the recorded tip positions (Fig. 6(b)). Maximum curvature is observed for a steering angle of 15°, resulting in a path with a radius of 200 mm. Since we are considering relatively small angles, we assume a linear relationship between the curvature and the steering angle. Performing a linear fit to the experimental curvatures results in a front frame offset of 55 mm (Fig. 6(b)). This value is used as an initial estimate in the parameter estimation. For steering angles larger than 7.5° the experimental curvatures show good agreement with the model. The needle paths for the smaller steering angles appear to become almost straight near the end, which explains the small curvatures.

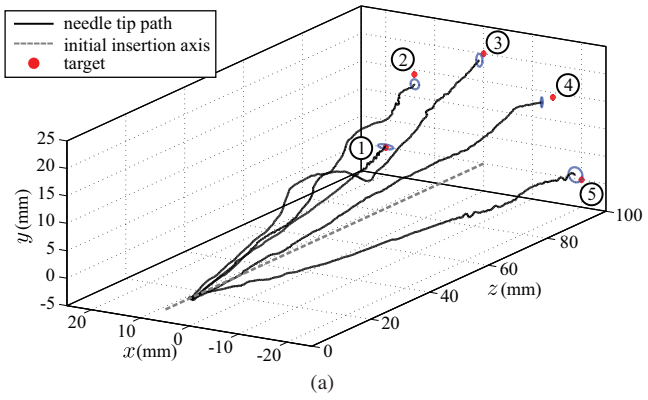

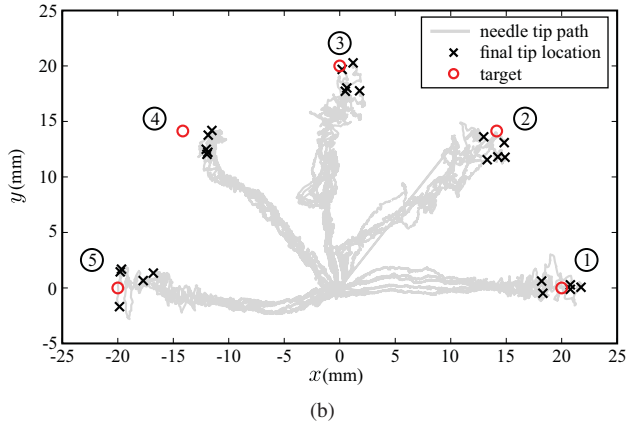

Fig. 8. The needle is steered towards different target locations ①-⑤ in the soft tissue phantom. All targets are located at a depth of 100 mm inside the phantom. Five insertions are performed for each target. (a) Three-dimensional view of the mean needle paths for each target. The blue ellipsoids indicate the standard deviation in final tip position. (b) Final tip locations and individual needle paths in the xy-plane. *The accompanying video demonstrates the results of these steering experiments.*

B. Parameter Estimation Experiments

In order to verify our proposed method for estimation of the front frame offset (l), we insert the needle into a multilayer phantom. This phantom consists of two gelatin layers: The first layer contains 14.9% gelatin and the second layer contains 8% gelatin. The needle is inserted at a steering angle of 20° with an insertion velocity of 5 mm/s. Estimation is performed for three different window lengths (W_t): 1 s, 3 s and 5 s (Fig. 7). The initial offset is set at 55 mm and estimation starts when the insertion has reached the length of the window. It can be seen that the offset increases when the needle enters the second layer of lower stiffness. This indicates that changes in phantom stiffness can be detected using our algorithm. A small window length of 1 s results in a noisy estimate of the offset compared to a large window length of 5 s. However, detecting the transition in stiffness between the different layers has a large delay for a large window size. Therefore, we choose a window size of 3 s for the steering experiments.

C. Needle Steering Experiments

We perform a set of experiments in which the needle is steered towards different target locations in the phantom. The needle is inserted with a constant velocity of 5 mm/s during all experiments. For practical reasons, a maximum angle of 30° is set for the steering angle. The phantom contains 14.9% gelatin and hence, before estimation an initial value of 55 mm is used for the front frame offset. Needle pose is determined from the FBG measurements during insertion, and actuated-tip orientation is calculated using the method described in Section II-B. The needle is steered towards five different target locations at 20 mm from the initial insertion axis at different orientations (Fig. 3). All targets are located at a depth of 100 mm in the phantom. Five insertions are performed for each target location. The needle tip paths and final tip positions are shown in Fig. 8. The targeting errors are presented in Table I. The mean, absolute targeting error for all insertions is 2.02 mm, with errors of 1.30 mm and 1.22 mm for the x-direction and y-direction, respectively. It can be seen that, for some insertions, the needle tip deviates from a straight path to the target (Fig. 8(b)). This can be caused by an initial misalignment of the needle prior to insertion. However, the controller is able to correct for this and steer the needle tip in the direction of the target.

TABLE I

TARGETING ERRORS OF THE STEERING EXPERIMENTS. MEAN ERRORS IN ARE PRESENTED ALONG WITH THEIR STANDARD DEVIATIONS (IN BRACKETS). ERRORS IN THE x-DIRECTION AND y-DIRECTION ARE DENOTED (I.E., ε_x AND ε_y) AS WELL AS THE NORM OF THE ERROR ($\|\varepsilon\|$). FOR EACH TARGET, FIVE INSERTIONS ARE PERFORMED. ALL REPORTED VALUES ARE IN MM.

Target	t_x	t_y	ε_x	ε_y	$\|\varepsilon\|$
1	20	0	1.36 (0.53)	0.31 (0.24)	1.41 (0.55)
2	14.14	14.14	0.71 (0.35)	1.77 (0.81)	2.02 (0.70)
3	0	20	0.87 (0.63)	1.42 (1.03)	1.78 (0.98)
4	-14.14	14.14	2.29 (0.20)	1.22 (0.94)	2.72 (0.28)
5	-20	0	1.24 (1.42)	1.37 (0.43)	2.15 (0.81)
all targets combined			1.30 (0.89)	1.22 (0.87)	2.02 (0.78)

V. CONCLUSIONS AND FUTURE WORK

In this study we have presented a novel needle design, consisting of a flexible needle with an actuated-tip which enables 3D steering through soft tissue. A new model for the needle is derived based on nonholonomic kinematics, which predicts the needle path based on the forward insertion velocity and actuated-tip orientation. We have presented a method for online parameter estimation during needle steering, which uses the kinematic model to estimate the front frame offset. This offset is related to the stiffness of the soft tissue, and hence allows to adapt the steering algorithm to changes in the soft tissue stiffness. Needle insertion experiments are done with a prototype needle (2 mm diameter) in soft-tissue simulants made from porcine gelatin. Results show a minimal bending radius of 200 mm. Steering experiments are done towards target locations at a depth of 100 mm in the phantom, located 20 mm from the initial insertion axis at different orientations. Mean targeting errors of 1.33 mm and 1.22 mm are observed in the x-direction and y-direction, corresponding to an absolute error of 2.02 mm.

Although the results of the steering experiments look promising, we believe they can be improved in future work. We did not take into account the compliance of the tendons, which prevented accurate control of the actuated-tip steering angle. Therefore, in future work we will model the tendon compliance. In this work we only considered point-to-point motion control of the needle towards a fixed target location. However, in future work we will use the kinematic model to design more advanced controllers which can be used to track a reference trajectory. This allows to plan the path before the insertion procedure, taking into account obstacle locations. Further, we plan to perform human-in-the-loop experiments, in which a human controls part of the needle insertion.

REFERENCES

[1] N. Abolhassani, R. V. Patel, and M. Moallem, "Needle insertion into soft tissue: A survey," *Medical Engineering and Physics*, vol. 29, no. 4, pp. 413–431, 2007.

[2] N. J. Cowan, K. Goldberg, G. S. Chirikjian, G. Fichtinger, R. Alterovitz, K. B. Reed, V. Kallem, W. Park, S. Misra, and A. M. Okamura, "Robotic needle steering: Design, modeling, planning, and image guidance," in *Surgical Robotics* (J. Rosen, B. Hannaford, and R. M. Satava, eds.), pp. 557–0582, Springer US, 2011.

[3] J. A. Engh, G. Podnar, D. Kondziolka, and C. N. Riviere, "Toward effective needle steering in brain tissue," in *Proceedings of the IEEE International Conference on Engineering in Medicine and Biology Society (EMBS)*, pp. 559–562, New York, USA, August 2006.

[4] G. J. Vrooijink, M. Abayazid, S. Patil, R. Alterovitz, and S. Misra, "Needle path planning and steering in a three-dimensional non-static environment using two-dimensional ultrasound images," *International Journal of Robotics Research (IJRR)*, vol. 33, no. 10, pp. 1361–1374, 2014.

[5] P. Sears and P. E. Dupont, "A steerable needle technology using curved concentric tubes," in *Proceedings of the IEEE International Conference of Intelligent Robots and Systems (IROS)*, pp. 2850–2856, October 2006.

[6] R. J. Webster, A. M. Okamura, and N. J. Cowan, "Toward active cannulas: Miniature snake-like surgical robots," in *Proceedings of the IEEE International Conference of Intelligent Robots and Systems (IROS)*, pp. 2857–2863, October 2006.

[7] S. Y. Ko, B. L. Davies, and F. Rodriguez y Baena, "Two-dimensional needle steering with a p̈rogrammable bevel ïnspired by nature: Modeling preliminaries," in *Proceedings of the IEEE International Conference of Intelligent Robots and Systems (IROS)*, pp. 2319–2324, October 2010.

[8] S. Y. Ko and F. Rodriguez y Baena, "Toward a miniaturized needle steering system with path planning for obstacle avoidance," *Transactions on Biomedical Engineering (TBME)*, vol. 60, pp. 910–917, April 2013.

[9] H. B. Gilbert and R. J. Webster, "Can concentric tube robots follow the leader?," in *Proceedings of the IEEE International Conference on Robotics and Automation (ICRA)*, pp. 4881–4887, Karlsruhe, Germany, May 2013.

[10] M. Abayazid, M. Kemp, and S. Misra, "3d flexible needle steering in soft-tissue phantoms using fiber bragg grating sensors," in *Proceedings of the IEEE International Conference on Robotics and Automation (ICRA)*, pp. 5843–5849, Karlsruhe, Germany, May 2013.

[11] R. J. Roesthuis, M. Kemp, J. J. van den Dobbelsteen, and S. Misra, "Three-dimensional needle shape reconstruction using an array of fiber bragg grating sensors," *IEEE/ASME Transactions on Mechatronics*, vol. 19, pp. 1115–1126, August 2014.

[12] S. Misra, K. B. Reed, B. W. Schafer, K. T. Ramesh, and A. M. Okamura, "Mechanics of flexible needles robotically steered through soft tissue," *International Journal of Robotics Research (IJRR)*, vol. 29, no. 13, pp. 1640–1660, 2010.

[13] A. Majewicz, S. P. Marra, M. G. van Vledder, M. Lin, M. A. Choti, D. Y. Song, and A. M. Okamura, "Behavior of tip-steerable needles in ex vivo and in vivo tissue," *Transactions on Biomedical Engineering*, vol. 59, pp. 2705–2715, October 2012.

[14] R. J. Webster, J. S. Kim, N. J. Cowan, G. S. Chirikjian, and A. M. Okamura, "Nonholonomic modeling of needle steering," *International Journal of Robotics Research (IJRR)*, vol. 25, no. 5-6, pp. 509–525, 2006.

[15] B. Siciliano, L. Sciavicco, L. Villani, and G. Oriolo, *Robotics: Modelling, Planning and Control*. Springer London, 2009.

[16] A. Othonos, K. Kalli, D. Pureaur, and A. Mugnier, *Optical Sciences*, ch. Fibre Bragg Gratings, pp. 189–262. Springer, 2006.

[17] R. J. Roesthuis, S. Janssen, and S. Misra, "On using an array of fiber bragg grating sensors for closed-loop control of flexible minimally invasive surgical instruments," in *Proceedings of the IEEE International Conference of Intelligent Robots and Systems (IROS)*, pp. 2545–2551, November 2013.

[18] A. Gefen and B. Dilmoney, "Mechanics of the normal woman's breast," *Technology and Health Care*, vol. 15, no. 4, pp. 259–271, 2007.

[19] R. J. Roesthuis, Y. R. van Veen, A. Jahya, and S. Misra, "Mechanics of needle-tissue interaction," in *Proceedings of the IEEE International Conference of Intelligent Robots and Systems (IROS)*, pp. 2557–2563, San Francisco, USA, September 2011.